

## Effect of phase composition on the formation of active sites in titania-ceria catalysts for ethyl acetate total oxidation

G.S. Issa<sup>1\*</sup>, M.D. Dimitrov<sup>1</sup>, D.G. Kovacheva<sup>2</sup>, J. Henych<sup>3</sup>, V. Štengl<sup>3</sup>, T.S. Tsoncheva<sup>1</sup>

<sup>1</sup>*Institute of Organic Chemistry with Centre of Phytochemistry, BAS, 1113 Sofia, Bulgaria*

<sup>2</sup>*Institute of General and Inorganic Chemistry, BAS, 1113 Sofia, Bulgaria*

<sup>3</sup>*Materials Chemistry Department, Institute of Inorganic Chemistry AS CR, Czech Republic*

Submitted on July 15, 2016; Revised on November 16, 2016

The aim of current investigation is to elucidate the effect of phase composition of titanium-cerium mixed oxides on their textural, structural and surface properties. Nanosized mesoporous TiO<sub>2</sub>-CeO<sub>2</sub> oxide materials were prepared by template-assisted hydrothermal synthesis using CTAB as a structure directing agent. The obtained samples were characterized by Nitrogen physisorption, X-ray diffraction, temperature-programmed reduction with hydrogen, UV-Vis, FTIR- and Raman spectroscopies. The catalytic activity of the obtained materials was tested in total oxidation of ethyl acetate as a representative member of hardly oxidized O-containing volatile organic compound (VOCs). All bi-component samples possess improved textural characteristics and redox properties due to the increased dispersion. All bi-component oxides demonstrate improved catalytic activity and selectivity in comparison with the mono-component materials in total oxidation of ethyl acetate. This could be a result of the improved textural characteristics and redox properties due to the increased particle dispersion.

**Keywords:** nanostructured metal oxides, ethyl acetate combustion.

### INTRODUCTION

Recently, volatile organic compounds (VOCs) have gained a significant contribution to air pollution [1], which makes the control of their emissions strongly imperative. Nowadays, there are numerous different methods for VOCs elimination such as adsorption, thermal oxidation and catalytic oxidation [1, 2]. Among them, the catalytic total oxidation has been recognized as more economically efficient process for VOCs elimination even at low concentrations, reducing also the level of toxic by-products emissions in a high extent [1–4]. Transition metal oxides are one of the alternatives to noble metal-containing catalysts due to their thermal stability, low cost and high catalytic activity [2,4]. Nanostructured metal oxides have been found to be very active, both in total and selective oxidation of hydrocarbons and their catalytic properties are related to the type of metal oxide species involved in the oxidation process [5, 6]. Besides, the use of a multicomponent system could enhance the catalyst performance due to the synergism that may occur between the components. Anatase-type titanium dioxide has been extensively used in environmental applications due to its high activity, chemical stability, robustness against photocorrosion, low toxicity and availability at low cost, especially for the detoxification of water and air [7, 8]. The surface properties of TiO<sub>2</sub> are primarily dependent

upon various factors such as particle size, structural defects/distortion and the presence of other dopants [7]. It is well known that the properties of metal oxide can be modified by the incorporation of another metal oxide to form mixed oxides at surface level. It was established that the doping of titania with different metal oxides could improve the redox properties of the obtained nanocomposites due to the appearance of interaction and/or synergism between the components [8]. Such modifications generate novel material properties, including higher catalytic activity in various reactions. Among the doping metals, cerium species have attracted particular attention due to their excellent redox chemistry and oxygen storage capacity [8, 9]. The catalytic properties of cerium reflect two features, which are the redox couple Ce<sup>4+</sup>-Ce<sup>3+</sup> with the ability of cerium to shift between CeO<sub>2</sub> and Ce<sub>2</sub>O<sub>3</sub> under oxidizing and reducing conditions, and the facile formation of labile oxygen vacancies with the relatively high mobility of bulk oxygen ions [9]. Recently, titania-ceria materials have been studied as good alternative for the oxidation catalysts and supports [8, 9]. Yang et al. [10] studied catalytic wet air oxidation (CWAO) of phenol over TiO<sub>2</sub>-CeO<sub>2</sub> catalysts. They observed an increase in the efficiency of the mixed materials due to the promoting effect of ceria in the structural and redox properties of titania. They found that the catalytic activity was seriously influenced by Ti/Ce mol ratio. A lot of data in the literature aimed on the highlighting of the relationship between the

\* To whom all correspondence should be sent:

E-mail: : issa@abv.bg

catalytic activity and the defective structure of these oxides.

The aim of current investigation is to study the catalytic behaviour of TiO<sub>2</sub>-CeO<sub>2</sub> materials as catalysts in volatile organic compounds oxidation using ethyl acetate as a probe molecule. On the base of a complex study with different methods, such as Nitrogen physisorption, XRD, Raman-, FTIR-, UV-Vis spectroscopy and temperature-programmed reduction with hydrogen, the effect of Ti/Ce ratio on the structural, textural and catalytic properties of the obtained binary oxides are discussed.

## EXPERIMENTAL

### Materials

Titania (TiO<sub>2</sub>) and ceria (CeO<sub>2</sub>) materials were synthesized by template-assisted technique using hexadecyl-N,N,N-trimethyl ammoniumbromide (CTAB) as a template, hydrothermal treatment at 373 K and calcination at 773 K according to procedure described in [11]. Similar synthesis was applied for the bi-component oxides, denoted as TiCe where the Ti/Ce mol ratio was 1:1, 1:2 and 2:1.

### Methods of characterization

Specific surface area (BET method) and total pore volume data were collected from nitrogen adsorption-desorption isotherms measured at 77 K using a Quantachrome NOVA 1200 apparatus. Powder X-ray diffraction patterns were collected on a Bruker D8 Advance diffractometer with Cu K $\alpha$  radiation using a LynxEye detector. FTIR spectra in the region of skeletal vibrations were recorded on a Bruker Vector 22 spectrometer at a resolution of 1–2 cm<sup>-1</sup>, accumulating 64–128 scans and KBr pellets technique. The UV-Vis spectra were recorded on a Jasco V-650 UV-Vis spectrophotometer equipped with a diffuse reflectance unit. Raman spectra were acquired with a DXR Raman microscope (Thermo Fischer Scientific, Inc., Waltham, MA) using a 780 nm laser. The TPR/TG analyses were performed on a Setaram TG92 instrument using a flow (100 cm<sup>3</sup> min<sup>-1</sup>) of 50 vol. % H<sub>2</sub> in Ar and a heating rate of 5 K min<sup>-1</sup>.

### Catalytic oxidation of ethyl acetate

The catalytic oxidation of ethyl acetate was performed in a flow type of microreactor, 0.030 g of the catalyst diluted with crash glass (weight ratio of 1:3), particle size of 0.3–0.6 mm and catalytic bed volume of about 0.5 cm with a mixture of ethyl acetate in air (1.21 mol %) and WHSV of 100 h<sup>-1</sup>. Before the catalytic activity experiments the samples were treated in argon at 373 K for 1 h. Gas chromatographic analyses were done on a HP 5890

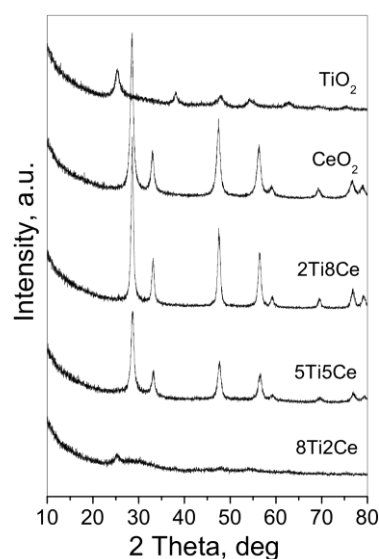
apparatus using carbon-based calibration. The products distribution was calculated as selectivities to CO<sub>2</sub> (S<sub>CO2</sub>), acetaldehyde (S<sub>AA</sub>), ethanol (S<sub>Et</sub>) and acetic acid (S<sub>AcAc</sub>) calculated by the equation:  $S_i = Y_i/X \cdot 100$ , where S<sub>i</sub> and Y<sub>i</sub> were the selectivity and the yield of (i) product and X was the conversion value.

## RESULTS AND DISCUSSION

In order to obtain information for the textural characteristics of the studied materials, nitrogen physisorption measurements are done (Table 1). According to IUPAC classification the acquired isotherms are of type IV, typical of materials with mesoporous structure (not shown) which could be expected when using CTAB as a structure-directing agent during synthesis and/or obtain a material comprised of nanosized particles. All obtained materials are characterized with high BET specific surface area and total pore volume. The addition of ceria to titania leads to an increase in the surface area and pore volume of the bi-component systems (Table 1). This effect is more pronounced for 8Ti2Ce sample. Note, that the BET surface area of all mixed oxide samples overcomes that one if the samples were mechanical mixtures of the individual oxides. This suggests interaction between the studied metal oxides.

**Table 1.** Nitrogen physisorption data and specific catalytic activity (T=600 K) of studied materials.

Sample	BET m <sup>2</sup> /g	Total Pore Volume ml/g	Specific catalytic activity (SA)
CeO <sub>2</sub>	46	0,26	1,76
TiO <sub>2</sub>	85	0,28	0,29
2Ti8Ce	55	0,29	1,01
5Ti5Ce	99	0,45	0,61
8Ti2Ce	166	0,62	0,39



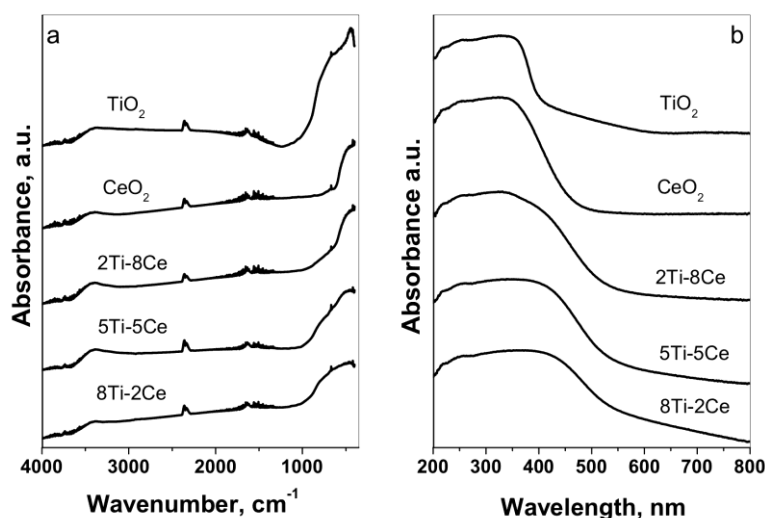
**Figure 1.** XRD patterns of TiO<sub>2</sub>, CeO<sub>2</sub> and TiCe materials.

Fig. 1 shows the X-ray diffraction patterns of titania-ceria materials. For pure  $\text{TiO}_2$ , only reflections of anatase titania ( $2\theta=25.6^\circ$ ,  $38.3^\circ$ ,  $47.8^\circ$  and  $62.5^\circ$ ) were detected [12] (Fig. 1, Table 2). In bi-component material with high titanium content (8Ti2Ce), the reflections of anatase are still present and no reflections of ceria are observed. With further increase of Ce content the former reflections become weaker and the wider. This indicates a decrease in the crystal size of  $\text{TiO}_2$  with the increase of Ce content in the samples (Table 2). This can be due to large lattice distortion resulting from the cerium addition. For pure  $\text{CeO}_2$ , the strong reflections are attributed to cubic fluorite-like

structure ( $2\theta = 28.5^\circ$ ,  $33.1^\circ$ ,  $47.5^\circ$ ,  $56.3^\circ$  and  $69.4^\circ$ ) [13]. For the Ce-rich sample (2Ti8Ce), no titanium oxide phases are detected. In this sample, the registered diffraction reflections are characteristic of cerianite  $\text{CeO}_2$  and they are slightly shifted to higher Bragg angles, which is due to a slight decrease of the ceria unit cell parameter (Table 2). Taking into account that the radius of  $\text{Ti}^{4+}$ -ion is  $0.74 \text{ \AA}$ , CN=6 and that one for  $\text{Ce}^{4+}$ -ion is  $0.97 \text{ \AA}$ , CN=6, the latter observation could be due to the incorporation of smaller  $\text{Ti}^{4+}$ -ions into the ceria lattice [14, 15]. However, the observed results are insufficient to assume formation of a solid solution with cerianite structure as was reported in [16].

**Table 2.** XRD data for  $\text{TiO}_2$ ,  $\text{CeO}_2$  and TiCe materials.

Sample	Space Group	Unit cell	Particles size, nm
<b>TiO<sub>2</sub></b>	Anatase, syn	3.7861	17.4
	Tetragonal – Body-centered I41/amd	9.493	
<b>CeO<sub>2</sub></b>	Cerium oxide	5.416	10.0
	Cubic - Face center - Fm-3m (225)		
<b>2Ti 8Ce</b>	Anatase, syn	5.409	17.0
	Tetragonal – Body-centered I41/amd		
	Cubic - Face center - Fm-3m (225)		
<b>5Ti5Ce</b>	Anatase, syn	3.782	< 5
	Tetragonal – Primitive P42/mnm (136)	9.514	
	Cerium oxide	5.403	
	Cubic - Face center - Fm-3m (225)		
<b>8Ti2Ce</b>	Anatase, syn	-	-
	Tetragonal – Primitive P42/mnm (136)	-	
	Cerianite (Ce), syn	-	
	Cubic - Face center - Fm-3m (225)	-	



**Figure 2.** FTIR spectra (a) and UV-Vis spectra (b) of  $\text{TiO}_2$ ,  $\text{CeO}_2$  and TiCe materials.

In order to obtain more information about the state of various metal oxide species, FTIR measurements were also done (Fig. 2a). For the pure TiO<sub>2</sub> sample, the peaks at 460, 620 and the shoulder at 910 cm<sup>-1</sup>, typical of anatase titania are registered (Fig. 2a) [14]. The broad and intensive band below 700 cm<sup>-1</sup> observed for the pure CeO<sub>2</sub> sample is related to the Ce–O bond vibrations. The band around 1600 cm<sup>-1</sup> is due to adsorbed water molecules [17]. The broad band in the interval 3100–3700 cm<sup>-1</sup> is assigned to O–H stretching vibrations. The variations in the intensity of these peaks in the FTIR spectra of the bi-component samples with cerium content implies that a possible interaction of ceria with titania provides differences in the surface defects, which reflects on the amount of surface hydroxyl groups and adsorbed water.

The diffuse reflectance UV-Vis spectra were further recorded (Fig. 2b), since this technique is

very sensitive to obtain more information for the environment of metal ions. The strong absorption feature in the UV-Vis spectrum of pure TiO<sub>2</sub> (Fig. 2b) at 350 nm is due to d-d electronic transition between Ti<sup>4+</sup>-ion and O<sup>2-</sup> ligand in anatase [18], which is consistent with the observation from XRD. The absorption in 300-500 nm range which is registered in the spectra of CeO<sub>2</sub> sample corresponds to Ce<sup>4+</sup>←O<sup>2-</sup> charge transfer (CT) [19]. The band at 250 nm could be due to the O<sup>2-</sup>→Ce<sup>3+</sup> CT transitions, which implies the occurrence of oxygen vacancy defects. In accordance with the XRD and nitrogen physisorption data, the observed changes in the 350–500 nm region for all bi-component materials confirm the assumption done above for the existence of strong interaction between the different metal ions and/or the increase in the metal oxides dispersion.

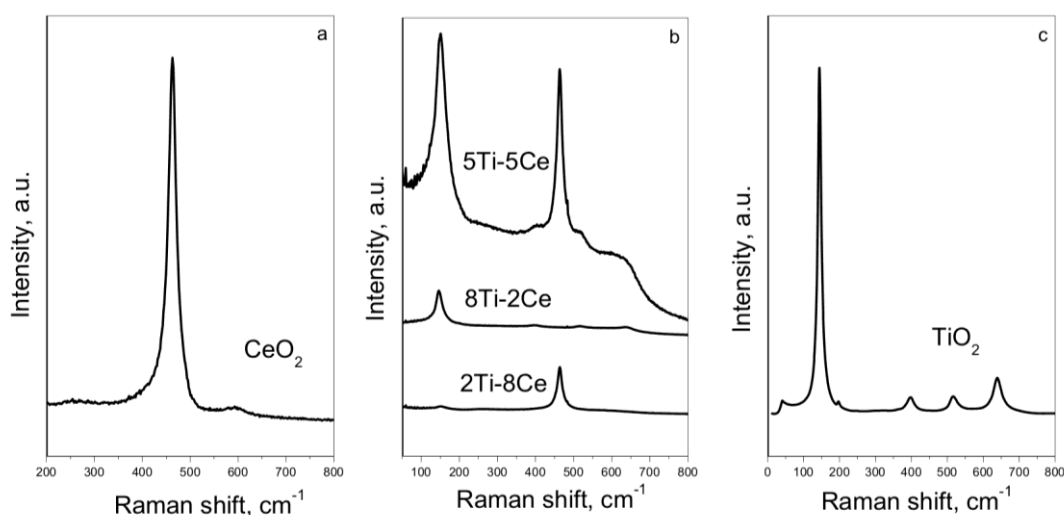


Figure 3. Raman spectra of CeO<sub>2</sub> (a), TiO<sub>2</sub> (b) and TiCe (c) materials.

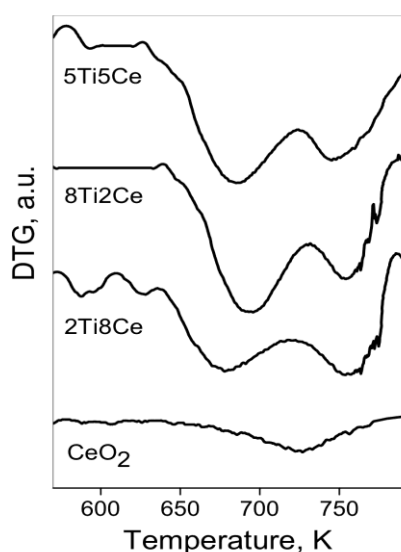


Figure 4. TPR–DTG profiles of TiO<sub>2</sub>, CeO<sub>2</sub> and TiCe materials.

In order to obtain more information for the type of interaction between the metal oxide nanoparticles, Raman spectra were recorded (Fig. 3). The spectrum of pure TiO<sub>2</sub> sample (Fig. 3c) presents the main peaks at 149, 198, 398, 515 and 644 cm<sup>-1</sup>, typical of anatase TiO<sub>2</sub> structure [20]. In case of the mixed samples, the observed decrease in the intensity of the main peak, typical of titanium oxide accompanied with its slight broadening could be due to particle size decrease, which is in accordance with the XRD data (Fig. 1, Table 2). The spectrum of CeO<sub>2</sub> consists of intense peak at 463 cm<sup>-1</sup>, which is assigned to F2g mode of CeO<sub>2</sub> fluorite structure (Fig. 3a) [21]. The appearance of an additional intense and weak broad band at about 600 cm<sup>-1</sup> is assigned to the formation of oxygen vacancies [15, 20]. For the bi-component materials, a slight shifting and broadening of the main Raman-active mode accompanied with a decrease

in its intensity is detected (Fig. 3b). This could be assigned to partial replacement of Ce ions with Ti ones, resulting in Ce-O bonds shortening and formation of smaller crystallites with defect structure. In the case of 8Ti2Ce sample, no peaks are observed for CeO<sub>2</sub>. According to XRD and UV-Vis data, we assign these effect to the improved metal oxide dispersion and/or the formation of mixed oxide phases.

Fig. 4 presents the TPR-DTG profiles of the samples treated in hydrogen. In case of pure ceria (Fig. 4), the registered weight loss corresponds to about 14 % reduction of Ce<sup>4+</sup> to Ce<sup>3+</sup>. The reduction effect for the bi-components samples is larger in comparison with pure CeO<sub>2</sub> and starts at lower temperature. In accordance with the physicochemical measurements, the observed effects indicate increased mobility of lattice oxygen. This effect is especially well pronounced for the sample with the lowest Ce content.

In Figure 5 is presented the evolution of the catalytic behaviour of mono- and bi-component materials in oxidation of ethyl acetate with time on stream at selected temperature (600 K). Beside CO<sub>2</sub> which is the most important product of ethyl acetate oxidation, ethanol (EtOH), acetaldehyde (AA) and acetic acid (AcAc) are also registered as by-products. The catalytic properties of pure CeO<sub>2</sub> remain almost unchanged during the whole investigated interval (Fig. 5), however, it exhibits low selectivity to ethyl acetate total oxidation (27 %), while ethanol (47%) is detected as the main by-product. At the same time, well defined tendency of a decrease in the catalytic activity after two hours of time-on-stream was observed for the pure TiO<sub>2</sub> sample that could be due to the release of hardly desorbable carbon based by-products (Fig. 5). The TiO<sub>2</sub> sample demonstrated high selectivity

to CO<sub>2</sub> in the first two hours of the reaction (Fig. 5b), and then the selectivity steeply decreased at the expense of by-products formation, mainly AA (25 %), EtOH (22 %) and ethane (18 %) at 600 K. No changes in the catalytic activity with time on stream are registered for all bi-component materials (Fig. 5a). Note that all bicomponent materials represent better catalytic activity than the corresponding mono-component ones. Taking into account the physicochemical data we assign this result to the considerable improvement in the textural characteristics of the mixed oxide materials and/or to the presence of more active mixed oxide phase. In order to ignore the effect of different specific surface area of the samples (Table 1), the specific catalytic activity was calculated as conversion at selected temperature (600 K) per unit surface area (Table 1). The obtained results demonstrate well defined tendency for specific activity increase with ceria content for the bi-component samples and extremely high value is observed for the pure CeO<sub>2</sub>. Thus the facilitated effect of doping of titania with cerium is not in simple relation with the increased specific surface area of metal oxides, as a result of the improved dispersion of the individual oxides. Moreover, TPR results clearly indicate presence of more readily reducible particles in bi-components materials (Fig. 4). In accordance with the XRD and Raman analyses, the improved reducibility of the mixed oxides could be due to the incorporation of Ti<sup>4+</sup> ions into the ceria lattice. This weakens the Ce-O bond and promotes the mobility of bulk oxygen in CeO<sub>2</sub>. As reported by Russo et al. [22], the lattice oxygen plays a crucial role in the VOCs oxidation catalysis *via* Mars-van Krevelen mechanism, which was also discussed for total oxidation of ethyl acetate [23].

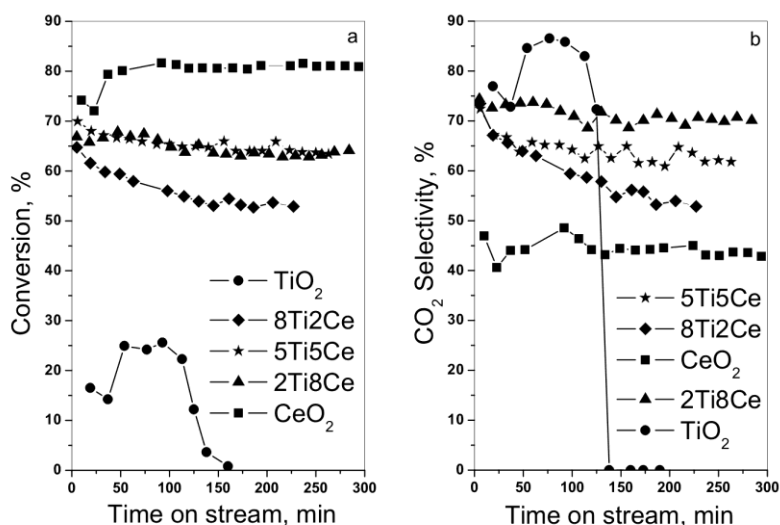


**Figure 5.** Ethyl acetate conversion (a) and selectivity to CO<sub>2</sub> (b) with time on stream at 600K of TiO<sub>2</sub>, CeO<sub>2</sub> and TiCe materials.

In conclusion, as compared to the mono-component materials, bi-component ones were characterized with higher dispersion, better textural parameters and improved redox properties. This affects the catalytic activity and selectivity of the samples in ethyl acetate combustion, which could be successfully controlled by the Ti/Ce ratio. The formation of these finely dispersed mixed oxide crystallites promotes ethyl acetate oxidation via Mars van Krevelen mechanism, where the release of lattice oxygen is of primary importance. The increase in the Ti/Ce ratio for these materials promotes the segregation of finely dispersed and easily reducible mixed oxide nanoparticles which has a beneficial effect on the catalytic activity. Further investigation is in progress.

### CONCLUSIONS

To obtain new insight into the structure–activity relationships for the titania-ceria mixed oxides, a series of mono-component and bi-component TiO<sub>2</sub>–CeO<sub>2</sub> samples with different Ti/Ce molar ratios have been synthesized. Well defined effect of metal oxide dispersion improvement is registered for all bi-component systems. The strong interaction between CeO<sub>2</sub> and TiO<sub>2</sub> as well as the crystallization of particles in the nanoscale obviously improve the redox properties of the TiO<sub>2</sub>–CeO<sub>2</sub> mixed oxides. All bi-component oxides demonstrate improvement in the catalytic activity and selectivity in comparison with the mono-component ones. In addition, the high specific surface area of CeO<sub>2</sub>–TiO<sub>2</sub> mixed oxides also play an important role in enhancing their catalytic performance in the total oxidation of ethyl acetate.

**Acknowledgements:** The authors thank the National Science Fund of Bulgaria (project DFNI 02/2/2014) for financial support.

### REFERENCES

1. C.Y. Lu, M.Y. Wey, L.I. Chen, *Appl. Catal. A: Gen.*, **325**, 163 (2007).
2. J. Okal, M. Zawadzki, *Appl. Catal. B: Environ.*, **89**, 22 (2009).
3. D. Delimaris, T. Ioannides, *Appl. Catal. B: Environ.*, **89**, 295 (2009).
4. P. Papaefthimiou, T. Ioannides, X.E. Verykios, *Appl. Therm. Eng.*, **18**, 1005 (1998).
5. F. Bertinchamps, C. Gregoire, E.M. Gaineaux, *Appl. Catal. B* **66**, 10 (2006).
6. Ch.-H. Wang, Sh.-Sh. Lin, Ch.-L. Chen, H.-Sh. Weng, *Chemosphere*, **64**, 503 (2006).
7. I.D. González, R.M. Navarro, W. Wen, N. Marinkovic, J.A. Rodríguez, F. Rosa, J.L.G. Fierro, *Catal. Today*, **149**, 372 (2010).
8. G. Schmid, M. Baumle, M. Greekens, I. Heim, C. Osemann, T. Sawatowski, *Chem. Soc. Rev.*, **28**, 179 (1999).
9. Li, F.B., Li, X.Z., Hou, M.F., Cheah, K.W., Choy, W.C.H., *Appl. Catal. A*, **285**, 181 (2005).
10. S. Yang, W. Zhu, J. Wang, Z. Chen, *J. Hazard. Mater.*, **153**, 1248 (2008).
11. T. Tsoncheva, L. Ivanova, D. Paneva, I. Mitov, C. Minchev, M. Fröba, *Micropor. Mesopor. Mater.*, **120**, 389 (2009).
12. M. Altomare, M.V. Dozzi, G.L. Chiarello, A.D. Paola, L. Palmisano, E. Selli, *Catal. Today*, **252**, 184 (2015).
13. B. Zhao, B. Shi, X. Zhang, X. Cao, Y. Zhang, *Desalination*, **268**, 55 (2011).
14. H. Nur, *Mater. Sci. Eng. B – Sol* **133**, 49 (2006).
15. S. Yuesong, Z. Dahai, Y. Bo, N. Songbo, Z. Shemin, *J. Rare Earths*, **30**, No. 5, 431 (2012).
16. M.F. Luo, J.C.L.S. Chen, J.Q. Lu, Z.C. Feng, C. Li, *Chem. Mater.*, **13**, 197 (2001).
17. P. Innocenzi, *J. Non-Cryst. Solids* **316**, 309 (2003).
18. I. Nitoi, P. Oancea, M. Raileanu, M. Crisan, L. Constantin, I. Cristea, *J. Ind. Eng. Chem.*, **21**, 677 (2015).
19. L. Katta, P. Sudarsanam, G. Thrimurthulu, B.M. Reddy, *Appl. Catal. B: Environ.*, **101**, 101 (2010).
20. T. Kidchob, P. Falcaro, P. Schiavuta, S. Enzo, P. Innocenzi, *J. Am. Ceram. Soc.*, **91**, 2112 (2008).
21. G. Vlaic, R.D. Monte, P. Fornasiero, E. Fonda, J. Kaspar, M. Graziani, *J. Catal.* **182**, 378 (1999).
22. M. Piumetti, S. Bensaid, N. Russo, D. Fino, *Appl. Catal. B*, **180**, 271 (2016).
23. P.-O. Larsson, A. Andersson, *Appl. Catal. B*, **24**, 175 (2000).

## ВЛИЯНИЕ НА ФАЗОВИЯ СЪСТАВ ВЪРХУ ФОРМИРАНЕТО НА АКТИВНИ ЦЕНТРОВЕ В ТИТАН-ЦЕРИЕВИ КАТАЛИЗАТОРИ ЗА ПЪЛНО ОКИСЛЕНИЕ НА ЕТИЛАЦЕТАТ

Г.С. Исса<sup>1\*</sup>, М. Д. Димитров<sup>1</sup>, Д. Г. Ковачева<sup>2</sup>, И. Хених<sup>3</sup>, В. Щенгъл<sup>3</sup>, Т. С. Цочева<sup>1</sup>

<sup>1</sup>Институт по органична химия с Център по фитохимия, БАН

<sup>2</sup>Институт по обща и неорганична химия, БАН

<sup>3</sup>Институт по неорганична химия, Чехия

Постъпила на 15 юли, 2016 г. коригирана на 16 ноември, 2016 г.

(Резюме)

Цел на настоящото изследване е да се изясни влиянието на състава на получените титан-церий смесени оксиди върху техните текстурни, структурни и повърхостни свойства. За целта са получени титан-церий смесени оксиди чрез хидротермален синтез в присъствието на органичен темплейт. Образците са характеризирани с различни физикохимични техники – физична адсорбция на азот, прахова рентгенова дифракция, дифузионно-отражателна ултравиолетова, инфрачервена и раман спектроскопии, както и температурно-програмирана редукция с водород. Каталитичната им активност е тествана в реакция на пълно окисление на етилацетат, като представител на трудноокисляемо O-съдържащо летливо органично съединение. Всички получени материали са добре кристални като бикомпонентните се характеризират с подобрени текстурни характеристики в сравнение с монокомпонентните оксиди, вследствие увеличаване дисперсността на изграждащите ги наночастици и техния значително по-голям поров обем. Показано е и наличие на взаимодействие между металните оксиди в смесените образци. Тези резултати благоприятстват каталитичното поведение на бикомпонентните образци в изследваната реакция и разкриват техния потенциал за елиминиране на токсични газови емисии.